






**Possible unconventional two-band superconductivity in MoTe<sub>2</sub>**

Jiawei Luo,<sup>1</sup> Yanan Li,<sup>1,2</sup> Jiawei Zhang <sup>1</sup>, Haoran Ji <sup>1</sup>, He Wang <sup>3</sup>, Jun-Yi Shan <sup>1</sup>, Canxun Zhang,<sup>1</sup> Cong Cai,<sup>1</sup> Jun Liu,<sup>4</sup> Yong Wang,<sup>4</sup> Yan Zhang,<sup>1</sup> and Jian Wang <sup>1,5,6,\*</sup>

<sup>1</sup>International Center for Quantum Materials, School of Physics, Peking University, Beijing 100871, China

<sup>2</sup>Department of Physics, Pennsylvania State University, University Park, Pennsylvania 16802, USA

<sup>3</sup>Department of Physics, Capital Normal University, Beijing 100048, China

<sup>4</sup>Center of Electron Microscopy, State Key Laboratory of Silicon Materials, School of Materials Science and Engineering, Zhejiang University, Hangzhou 310027, China

<sup>5</sup>CAS Center for Excellence in Topological Quantum Computation, University of Chinese Academy of Sciences, Beijing 100190, China

<sup>6</sup>Beijing Academy of Quantum Information Sciences, Beijing 100193, China



(Received 31 October 2019; revised 12 July 2020; accepted 13 July 2020; published 4 August 2020)

The coexistence of the type-II Weyl semimetal phase and superconductivity in the layered transition-metal dichalcogenide MoTe<sub>2</sub> is of great interest as it is considered a promising candidate for an intrinsic topological superconductor. However, the ultralow superconducting critical temperature ( $T_c$ ) of  $\sim 0.1$  K limits the exploration of the intrinsic superconducting properties. Here the superconductivity in MoTe<sub>2</sub> is investigated by systematic ultralow temperature transport measurements with standard four-electrode configuration, together with the hard point-contact (PC) technique which can enhance the  $T_c$  and detect the *in situ* spectroscopic information of the pairing symmetry. The temperature dependence of the superconducting critical field from transport measurements and the two-step double conductance peaks from the PC spectra measurements both suggest the two-band superconductivity in MoTe<sub>2</sub>. Together with the occasional observation of zero-bias conductance peaks in the spectra, our results suggest the unconventional two-band superconductivity with potential  $s_{+-}$  pairing in MoTe<sub>2</sub>.

DOI: [10.1103/PhysRevB.102.064502](https://doi.org/10.1103/PhysRevB.102.064502)

The layered transition-metal dichalcogenides (TMDs) have attracted tremendous attention worldwide owing to their rich physical properties such as the exhibition of quantum spin Hall effect [1,2], charge density wave [3], Weyl semimetal phase [4], superconductivity [5], unsaturated magnetoresistance [6], in addition to promising applications in nanoscale van der Waals devices [7]. As a typical TMD material,  $T_d$  phase MoTe<sub>2</sub> has been extensively studied. Band-structure calculations [8,9], angle-resolved photoemission spectroscopy (ARPES) [10–13] and quasi-particle interference experiments [14] show the existence of Fermi arc surface states and Weyl points in this material, suggesting  $T_d$  phase MoTe<sub>2</sub> is a type-II Weyl semimetal. Compared to another typical type-II Weyl semimetal WTe<sub>2</sub> [4,15–17], MoTe<sub>2</sub> shows a larger momentum separation of the Weyl points and a larger size of the topological Fermi arcs, which are easier to be resolved and studied. More interestingly, transport measurements reveal the superconductivity properties of this material [5]. As a rare example that possesses both superconducting phase and topologically nontrivial band structure, MoTe<sub>2</sub> is considered a promising candidate for intrinsic topological superconductor. This makes investigations of superconductivity in MoTe<sub>2</sub> very interesting since the surface or edge of a topological superconductor can host Majorana quasiparticles or Majorana zero modes (MZMs),

which obey non-Abelian statistics and can be used in fault-tolerant quantum computations [18,19]. Nevertheless, the  $T_c$  of intrinsic bulk MoTe<sub>2</sub> is only 0.1 K [5], hindering the exploration of potential topological superconductivity (TSC) therein.

Since it is not easy to investigate the intrinsic superconducting properties of MoTe<sub>2</sub>, previous experimental efforts are mainly focused on the enhanced superconductivity through high pressure or doping methods. The  $T_c$  is remarkably enhanced by pressure and a dome-shaped superconducting phase in pressure-temperature diagram is observed with a maximum  $T_c$  of 8.2 K at 11.7 GPa [5]. Similar enhancements of  $T_c$  are observed in *S*-, *Se*- and *Re*-doped MoTe<sub>2</sub> as well as *Te*-deficient MoTe<sub>2</sub> with a maximum  $T_c$  of  $\sim 4$  K [20–24]. Both high-pressure and doping measurements on MoTe<sub>2</sub> show signatures of two-band superconductivity with the possible  $s_{+-}$  pairing [24,25]. Note that the superconductor MoTe<sub>2</sub> represents a time-reversal-invariant Weyl semimetal, which has four pairs of topologically nontrivial Weyl points at the boundary of electron and hole pockets. Thus, the possible  $s_{+-}$  pairing in MoTe<sub>2</sub> may lead to the TSC as the TSC is predicted in time-reversal-invariant Weyl semimetals with the sign change of the superconducting gap function between Fermi surfaces with opposite Chern numbers [26]. However, the evidence of the possible  $s_{+-}$  pairing in pristine MoTe<sub>2</sub> is still missing. In this paper, we report our standard four-electrode ultralow temperature measurements on the intrinsic superconducting MoTe<sub>2</sub> bulk-crystal, which

\*Corresponding author: [jianwangphysics@pku.edu.cn](mailto:jianwangphysics@pku.edu.cn)

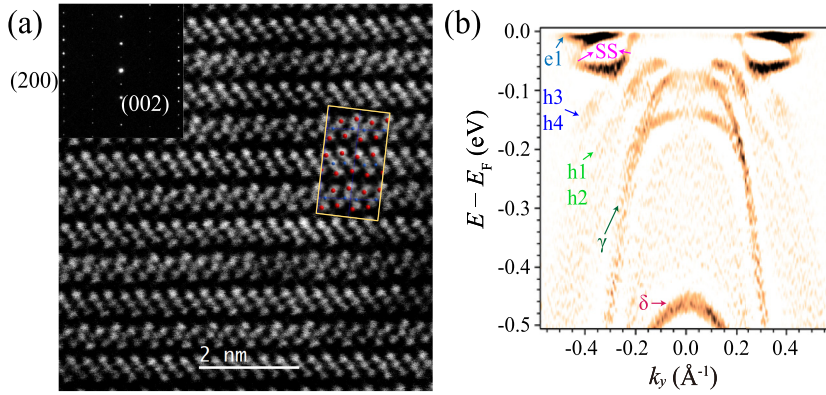


FIG. 1. Structural and topological properties of MoTe<sub>2</sub>. (a) The atomically resolved HAADF STEM image of MoTe<sub>2</sub> sample taken along the (010) crystalline direction. Inset is the electron diffraction patterns along (010) crystalline direction. The red and blue spheres in the yellow rectangle represent Te and Mo atoms, respectively. (b) The intensity plot of the photoemission spectra along the  $\Gamma$ -X direction, with the bulk conduction band, bulk valence band, and surface states indicated.

give the transport evidence of two-band superconductivity with stronger interband coupling than intraband coupling, supporting  $s_{+-}$  pairing. The two-band superconductivity is confirmed by the point-contact spectroscopy (PCS) results showing the two-step double conductance peaks structure. The occasional zero-bias conductance peak (ZBCP) features in the PCS represent the Andreev bound states (ABSs) resulting from the  $\pi$ -phase shift of internal phase from the order parameter in superconductors, suggesting the unconventional two-band superconductivity with potential  $s_{+-}$  pairing.

MoTe<sub>2</sub> single crystals were grown by vapor transport method using iodine as the transport agent in a two-zone tube furnace [20,24,27]. The standard four-electrode resistance measurements were conducted in a dilution refrigerator based on 16-T Physical Property Measurement System (16 T PPMS, Quantum Design). The low-temperature point-contact measurements were carried out in a Leiden dilution refrigerator (CF450). The point-contact spectroscopic results exhibited as the normalized differential conductance versus the bias voltage ( $dI/dV$  vs  $V$ ) were acquired from the junctions formed between a normal metal or ferromagnetic tip and the superconducting MoTe<sub>2</sub> sample. Our samples are mounted on the piezo steppers from the Attocube which can move in three directions. The copper housing which contains the steppers and the tip holder is cooled down in the dilution refrigerator (CF450) to maintain temperature equilibrium between the tip and sample. More details can be found in the Supplemental Material (SM) [28].

First, the scanning transmission electron microscopy (STEM) and the ARPES measurements are exerted to characterize the structural and topological properties of our MoTe<sub>2</sub> sample. Figure 1(a) is a high angle annular dark-field (HAADF) Z-contrast image from STEM, which shows the atomic arrangement of Mo and Te (the red and blue spheres in the yellow rectangle represent Te and Mo atoms, respectively) and demonstrates the crystal structure of our MoTe<sub>2</sub> sample. The upper inset is the diffraction pattern of the [010] direction. As shown in Fig. 1(b), the intensity plot of the photoemission spectra along the  $\Gamma$ -X direction exhibits the bulk valence band ( $h1$ ,  $h2$ ,  $h3$ , and  $h4$ ), Fermi arc surface states (SSs), and bulk conduction band ( $e1$ ) as indicated, which is consistent with the previous reported results on Weyl semimetal MoTe<sub>2</sub> [10,12]. Both the STEM and the ARPES results confirm the high quality of our sample.

The inset of Fig. 2(a) is the temperature dependence of four-electrode resistance  $R(T)$  from 300 to 1.8 K at zero field and 150 kG under the cooling and warming modes, showing an anomaly with hysteresis around 250 K which is associated with the structural phase transition from the  $17'$  to the  $T_d$  phase [5]. The  $R(T)$  curve in Fig. 2(a) shows a clear superconducting transition with an onset  $T_c$  around 154 mK, indicated by extrapolating both the normal-state resistance and the superconducting transition curve, and zero resistance  $T_c$  below 100 mK. To further explore the superconductivity of intrinsic MoTe<sub>2</sub>, four-electrode resistance as a function of magnetic field at different temperatures is systematically measured in the ultralow temperature regime with the field direction perpendicular [Fig. 2(b)] and parallel [Fig. 2(c)] to the sample (001) surface. The temperature dependence of the upper superconducting critical field  $\mu_0 H_{c2}$  (defined as the average of the two values at positive and negative magnetic fields required to reach 50% of the normal state resistance) in the perpendicular direction is shown in Fig. 2(d), which exhibits a good agreement with the phenomenological Werthamer-Helfand-Hohenberg (WHH) expression for two-band superconductors [29] (the solid line). In a two-band WHH model, the upper critical field  $\mu_0 H_{c2}$  can be described with the following formula [24]:

$$\begin{aligned}
 & a_0[\ln t + U(h)][\ln t + U(\eta h)] + a_2[\ln t + U(\eta h)] \\
 & + a_1[\ln t + U(h)] = 0, \\
 & t = \frac{T}{T_c}, \quad U(x) = \psi\left(\frac{1}{2} + x\right) - \psi\left(\frac{1}{2}\right), \\
 & \eta = \frac{D_2}{D_1}, \quad h = \frac{\hbar\mu_0 H_{c2} D_1}{2\varphi_0 k_B T}, \quad a_0 = \frac{2\varpi}{\lambda_0}, \quad a_1 = 1 + \frac{\lambda_-}{\lambda_0}, \\
 & a_2 = 1 - \frac{\lambda_-}{\lambda_0}, \\
 & \varpi = \lambda_{11}\lambda_{22} - \lambda_{12}\lambda_{21}, \quad \lambda_0 = \sqrt{\lambda_-^2 + 4\lambda_{12}\lambda_{21}}, \\
 & \lambda_- = \lambda_{11} - \lambda_{22}.
 \end{aligned}$$

$\psi(x)$  is the digamma function.  $D_1$  and  $D_2$  are intraband diffusivities of bands 1 and 2, while  $\varphi_0$  stands for magnetic flux quantum. Fitting parameters include intraband coupling strength  $\lambda_{11}$ ,  $\lambda_{22}$ , interband coupling strength  $\lambda_{12}$ ,  $\lambda_{21}$  and

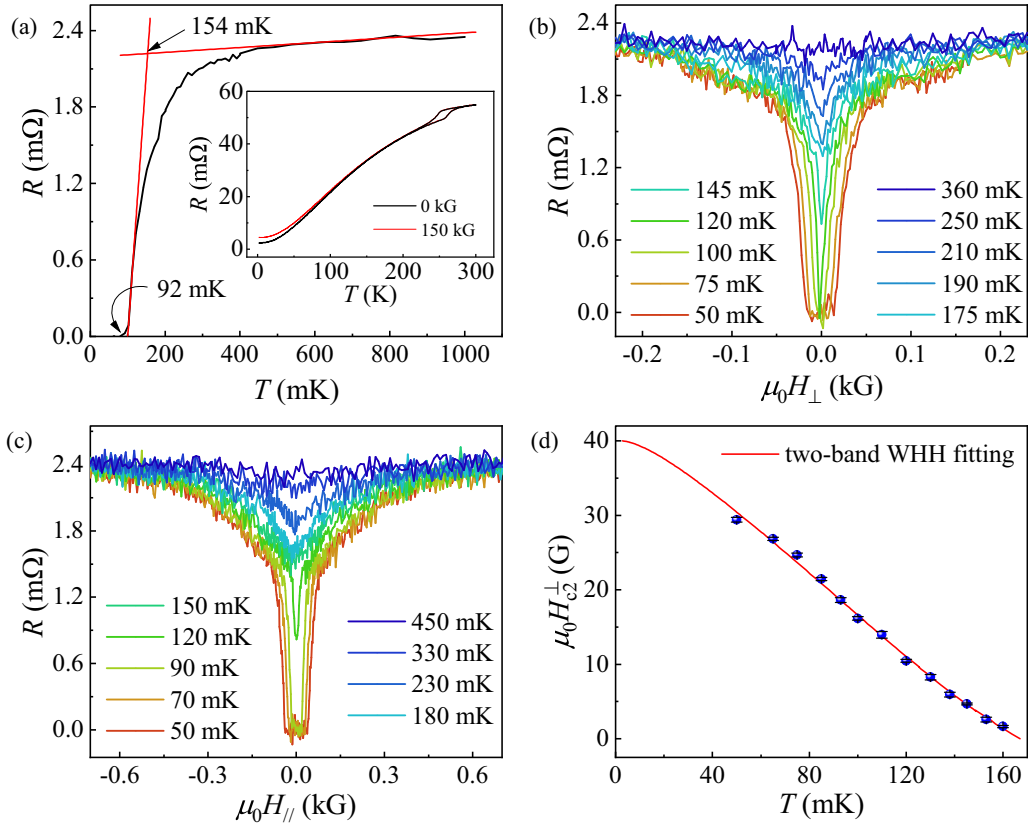


FIG. 2. Superconducting properties of the MoTe<sub>2</sub>. (a) Temperature dependence of four-electrode resistance at zero field showing the onset  $T_c$  around 154 mK (defined by extrapolating both the normal state resistance and the superconducting transition curve). Inset: Temperature dependence of four-probe resistance from 1.8 to 300 K at different perpendicular magnetic fields, showing the structural phase transition loop around 250 K. (b), (c) Magnetic field dependence of four-electrode resistance at different temperatures with the magnetic field perpendicular and parallel to the sample (001) surface. (d) Temperature dependence of perpendicular upper critical field  $\mu_0 H_{c2}^{\perp}$  (defined as the magnetic field required to reach 50% of the normal-state resistance). The solid line is the two-band WHH fitting curve.

diffusivities  $D_1$  and  $D_2$ . The fitting details can be found in the SM [28]. The fitting result  $\varpi$  is  $-2.30 < 0$ , which means a stronger interband coupling than intraband coupling [30,31], favoring possible  $s_{+-}$  superconductivity than conventional  $s_{++}$  pairing. Note that the doping and high-pressure studies on MoTe<sub>2</sub> also suggest  $s_{+-}$  superconductivity [24,25].

To further reveal the superconducting properties of MoTe<sub>2</sub>, systematic hard PC measurements were carried out with four kinds of tips (nonmagnetic Au, PtIr, W, and ferromagnetic Ni). Similar to high-pressure and doping experimental results on MoTe<sub>2</sub> [5,24], the  $T_c$  is significantly enhanced from 0.1 K to the highest 4.26 K by the tip point contact. The spectra can mainly be categorized into two types: one with double conductance peaks (DCPs) feature reflecting the normal Andreev reflection and the other with a ZBCP feature accompanied by dips on its sides.

The spectra in Figs. 3(a) and 3(b) acquired with a normal-metal Au tip show two obvious conductance peaks and multiple conductance dips that are symmetric about the zero bias. The DCPs (located at  $\pm 0.6$  meV at 0.5 K) and the multiple conductance dips are signatures of the superconductivity, which can be suppressed at temperature near 4.5 K or a perpendicular magnetic field of 8 kG at 1.0 K (regarded as  $\mu_0 H_c$ ). The DCPs are typical spectroscopic features indicating the gap energy of conventional or unconventional supercon-

ductors in the normal-metal/superconductor junctions resulted from the Andreev reflection [32]. Interestingly, a new step feature appears at higher magnetic fields of 3.0, 5.0, and 6.0 kG [Fig. 3(a)]. This new step feature is a typical evidence of multiband superconductivity, which has also been reported in two-band superconductors like  $s_{++}$  MgB<sub>2</sub> [33] and  $s_{+-}$  Ba(Fe<sub>1.92</sub>Co<sub>0.08</sub>)<sub>2</sub>As<sub>2</sub> [34]. The invisibility of the new step feature at low temperatures and fields can be attributed to the small proportion of the related superconducting component. The multiple conductance dips at large bias might be signatures of the different superconducting critical currents [35]. The two-band superconductivity is more clearly observed in Figs. 3(c) and 3(d) by a ferromagnetic Ni tip. In these two figures, the spectra show distinguished two-step features at 0.5 K with zero fields. Both steps disappear when temperature increases to 2.6 K or perpendicular magnetic field reaches 5.0 kG at 0.5 K. The spectra with two-step features can be roughly fitted by the extended  $s_{+-}$  BTK model in multiband superconductors [36] (see the SM [28]), supporting the two-band  $s_{+-}$  superconductivity in MoTe<sub>2</sub>. A more detailed and complex modeling considering the Fermi-surface topology and the symmetry of the order parameters is still desired for the topological Weyl superconductor MoTe<sub>2</sub> to convincingly prove the  $s_{+-}$  symmetry, like the three-dimensional (3D) extended BTK model for Fe-based superconductors [37].

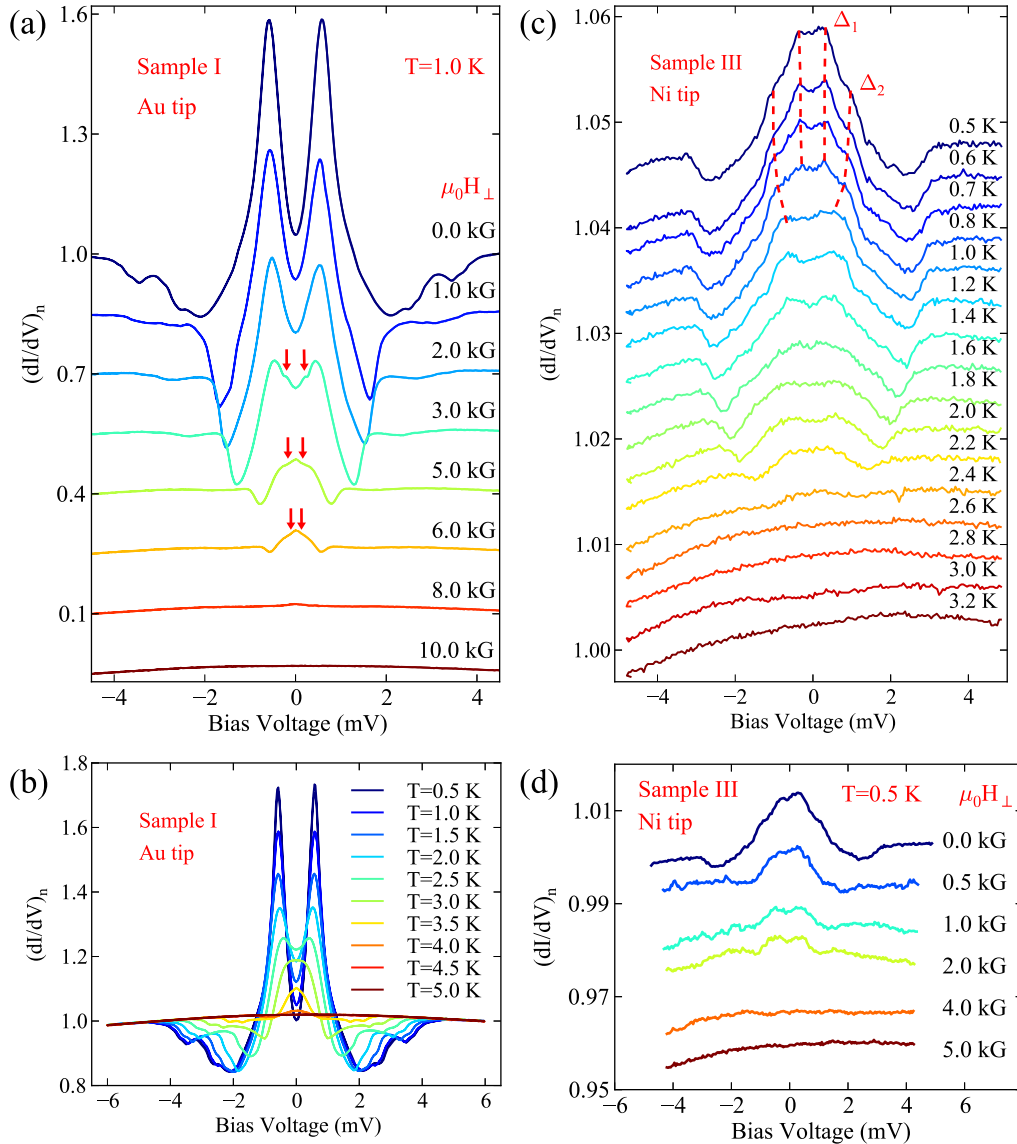


FIG. 3. PCS of enhanced superconductivity with two-band pairing in MoTe<sub>2</sub> samples. (a) Magnetic field dependence of the normalized  $dI/dV$  spectra on MoTe<sub>2</sub> sample I with a gold tip, showing steplike feature at 3.0, 5.0, and 6.0 kG marked with red arrows. (b) Temperature dependence of the normalized  $dI/dV$  spectra on MoTe<sub>2</sub> sample I with a gold tip. (c), (d) Temperature and magnetic field dependence of the normalized  $dI/dV$  spectra showing steplike features on MoTe<sub>2</sub> sample III with a nickel tip. Proper shifts have been made in (a), (c), and (d) for clarity.

Another type of spectra with an obvious ZBCP indicating the ABSs are observed by using both nonmagnetic tips and ferromagnetic Ni tips as shown in Figs. 4(a) and 4(b). Both DCPs and ZBCPs with the energy scale of 0.3 meV are observed in spectra at different contact points and by different types of tips as exhibited in Fig. 4(c), suggesting that the conductance dips accompany with the ZBCP are not critical current dips but signatures with an energy scale in proximity to the superconducting gap since the locations of critical current dips depend on the PC resistances [35]. The ZBCP does not split at the lowest temperature or under magnetic fields, which is at odds with the BTK theory for conventional Andreev reflection [32,38] or the magnetic scattering [39] respectively. The ZBCP can even survive at high magnetic field until the superconductivity is totally suppressed, which is against the reflectionless tunneling [40,41] process. A

statistic result of spectra from 45 different point contact states in Fig. 4(d) indicates that the energy scale of ZBCP feature (observed in seven cases) is around 0.3 meV, in proximity to the smaller gap  $\Delta_1$  shown in Fig. 3(c). The ZBCP accompanied by conductance dips with an energy scale of superconducting gap can be theoretically explained by unconventional ABSs originating from the  $\pi$ -phase shift of internal phase of the order parameter in unconventional superconductors [42,43]. Thus our PCS results suggest MoTe<sub>2</sub> as a two-band superconductor with unconventional ABSs, consistent with  $s_{+-}$  superconductivity raised in Fig. 2 as the sign change of the wave function of two bands in  $s_{+-}$  superconductors may also lead to mid-gap ABSs [36].

Considering the lack of an inversion center in the unit cell [9], mixed pairing states may exist in MoTe<sub>2</sub> and other unconventional pairing mechanisms cannot be completely ex-

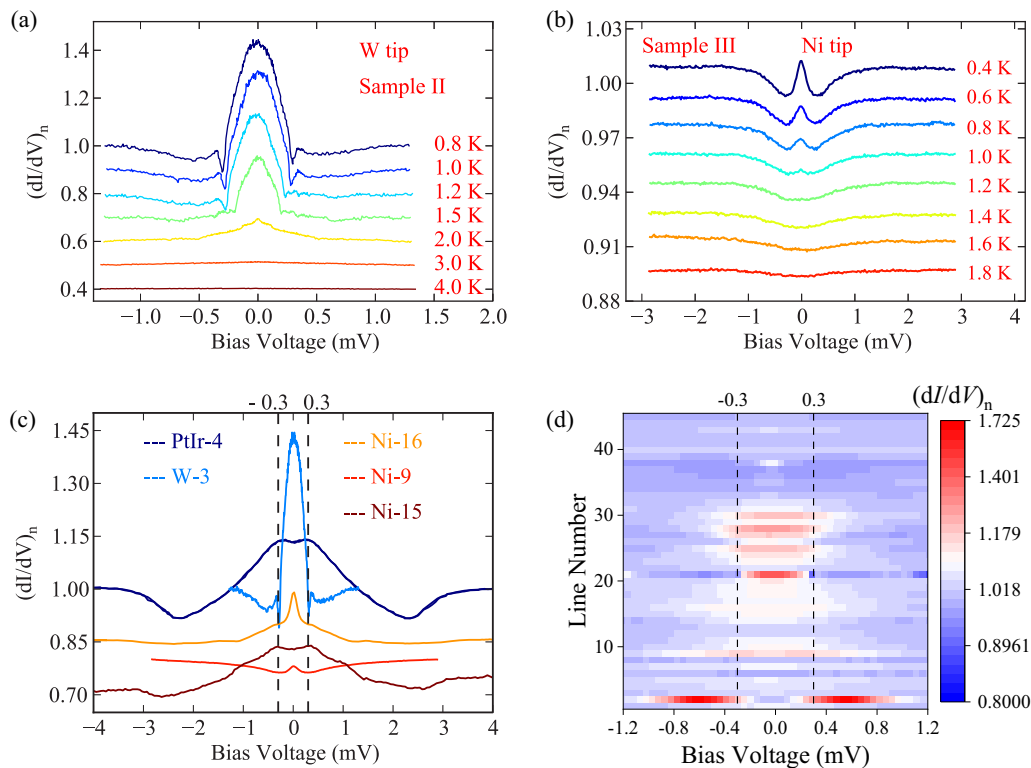


FIG. 4. Spectra with ZBCP and conductance dips of typical energy value of 0.3 mV on MoTe<sub>2</sub> samples. (a) Temperature dependence of the normalized  $dI/dV$  spectra showing the ZBCP feature on MoTe<sub>2</sub> sample II with a tungsten tip. (b) Temperature dependence of the normalized  $dI/dV$  spectra showing the ZBCP feature on MoTe<sub>2</sub> sample III with a nickel tip. (c) Spectra with double conductance peaks or a ZBCP with the typical energy value of 0.3 mV on MoTe<sub>2</sub> by different types of tips. The spectrum labeled “Ni-15” is from Fig. 3(c) but the conductance enhancement is 20-fold enlarged for clarity. (d) A statistic result of spectra from 45 point-contact states showing 0.3 mV as a characteristic value. Proper shifts have been made in (a), (b), and (c) for clarity.

cluded. However, as shown in spectra with a ferromagnetic Ni tip, the critical temperature  $T_c$  is suppressed under a ferromagnetic tip comparing to a normal metal tip, which suggests that the triplet superconductivity is not likely to be dominant. Density functional theory calculations reveal that the topological Weyl state of MoTe<sub>2</sub> persists under pressure [44]. The “gaplesslike” ZBCP has also been reported by a soft PC measurement [45] hinting a topological superconducting state on the MoTe<sub>2</sub> surface. Thus, our PCS results of two-band superconductivity with surface ABSs in MoTe<sub>2</sub> are reasonable and the observations of possible  $s_{+-}$  superconductivity in the time-reversal invariant Weyl semimetal MoTe<sub>2</sub> support the potential topological superconductivity [26]. Besides, as calculated in a nodeless  $s_{+-}$  model [36], a zero-energy bound state appears only when the two energy gap  $\Delta_1$ ,  $\Delta_2$ , and the mixing coefficient  $\alpha$  follow the relation  $\alpha^2 = \Delta_1/\Delta_2$ . [ $\alpha = \alpha_0\phi_q(0)/\phi_p(0)$ ,  $\alpha_0$  is the ratio of probability amplitudes for an electron in the normal metal tunneling into the second band of the superconductor,  $p$  and  $q$  are the Fermi vectors for the two bands,  $\phi$  is the Bloch function in the two-band superconductor.] This relation is hard to satisfy. However, in our point-contact experiments, seven spectra from 45 different point-contact states show the ZBCP feature indicating the zero-energy bound state. Thus, a nodal  $s_{+-}$  pairing could be more likely in MoTe<sub>2</sub> according to our experimental results.

As a result, the two-band superconductivity is proved in MoTe<sub>2</sub> as the  $\mu_0H_{c2}$ - $T$  phase diagram from our ultralow

temperature study follows the relation of two-band WHH theory. The two-band superconductivity of MoTe<sub>2</sub> is further confirmed by the PCS results showing a two-step DCPs structure exhibiting the two superconducting gaps. Considering the two-band WHH fitting with the strong interband coupling and the ZBCP feature in the PCS originating from the formation of zero-energy ABSs, our measurements suggest the unconventional two-band superconductivity with possible  $s_{+-}$  pairing on type-II Weyl semimetal MoTe<sub>2</sub>, supporting potential topological superconductivity in MoTe<sub>2</sub>.  $s_{+-}$  superconductivity is believed to exist in most of the iron-based superconductors with strong interband electron-hole Coulomb repulsion interaction [30]. Further investigations on the origin of  $s_{+-}$  pairing in nonmagnetic topological Weyl superconductor MoTe<sub>2</sub> are highly desired.

The authors acknowledge Z. Wang and W. Han for helpful discussions. This work was financially supported by the National Key Research and Development Program of China (Grants No. 2018YFA0305600 and No. 2017YFA0303302), the National Natural Science Foundation of China (Grants No. 11888101, No. 11774008 and No. 11704279), the Strategic Priority Research Program of Chinese Academy of Sciences (Grant No. XDB28000000), and Beijing Natural Science Foundation (Grant No. Z180010).

J.L. and Y.L. contributed equally to this work.

- [1] X. Qian, J. Liu, L. Fu, and J. Li, Quantum spin Hall effect in two-dimensional transition metal dichalcogenides, *Science* **346**, 1344 (2014).
- [2] S. Tang, C. Zhang, D. Wong, Z. Pedramrazi, H.-Z. Tsai, C. Jia, B. Moritz, M. Claassen, H. Ryu, S. Kahn, J. Jiang, H. Yan, M. Hashimoto, D. Lu, R. G. Moore, C.-C. Hwang, C. Hwang, Z. Hussain, Y. Chen, M. M. Ugeda *et al.*, Quantum spin Hall state in monolayer  $1T'$ -WTe<sub>2</sub>, *Nat. Phys.* **13**, 683 (2017).
- [3] D.W. Shen, B. P. Xie, J. F. Zhao, L. X. Yang, L. Fang, J. Shi, R. H. He, D. H. Lu, H. H. Wen, and D. L. Feng, Novel Mechanism of a Charge Density Wave in a Transition Metal Dichalcogenide, *Phys. Rev. Lett.* **99**, 216404 (2007).
- [4] A. A. Soluyanov, D. Gresch, Z. Wang, Q. S. Wu, M. Troyer, X. Dai, and B. A. Bernevig, Type II Weyl semimetals, *Nature (London)* **527**, 495 (2015).
- [5] Y. Qi, P. G. Naumov, M. N. Ali, C. R. Rajamathi, W. Schnelle, O. Barkalov, M. Hanfland, S.-C. Wu, C. Shekhar, Y. Sun, V. Süß, M. Schmidt, U. Schwarz, E. Pippel, P. Werner, R. Hillebrand, T. Förster, E. Kampert, S. Parkin, R. J. Cava *et al.*, Superconductivity in Weyl semimetal candidate MoTe<sub>2</sub>, *Nat. Commun.* **7**, 11038 (2016).
- [6] M. N. Ali, J. Xiong, S. Flynn, J. Tao, Q. D. Gibson, L. M. Schoop, T. Liang, N. Haldolaarachchige, M. Hirschberger, N. P. Ong, and R. J. Cava, Large, non-saturating magnetoresistance in WTe<sub>2</sub>, *Nature (London)* **514**, 205 (2014).
- [7] Y. Liu, N. O. Weiss, X. Duan, H.-C. Cheng, Y. Huang, and X. Duan, Van der Waals heterostructures and devices, *Nat. Rev. Mater.* **1**, 16042 (2016).
- [8] Y. Sun, S.-C. Wu, M. N. Ali, C. Felser, and B. Yan, Prediction of Weyl semimetal in orthorhombic MoTe<sub>2</sub>, *Phys. Rev. B* **92**, 161107(R) (2015).
- [9] Z. Wang, D. Gresch, A. A. Soluyanov, W. Xie, S. Kushwaha, X. Dai, M. Troyer, R. J. Cava, and B. A. Bernevig, MoTe: a Type-II Weyl Topological Metal, *Phys. Rev. Lett.* **117**, 056805 (2016).
- [10] K. Deng, G. Wan, P. Deng, K. Zhang, S. Ding, E. Wang, M. Yan, H. Huang, H. Zhang, Z. Xu, J. Denlinger, A. Fedorov, H. Yang, W. Duan, H. Yao, Y. Wu, S. Fan, H. Zhang, X. Chen, and S. Zhou, Experimental observation of topological Fermi arcs in type-II Weyl semimetal MoTe<sub>2</sub>, *Nat. Phys.* **12**, 1105 (2016).
- [11] L. Huang, T. M. McCormick, M. Ochi, Z. Zhao, M.-T. Suzuki, R. Arita, Y. Wu, D. Mou, H. Cao, J. Yan, N. Trivedi, and A. Kaminski, Spectroscopic evidence for a type II Weyl semimetallic state in MoTe<sub>2</sub>, *Nat. Mater.* **15**, 1155 (2016).
- [12] A. Tamai, Q. S. Wu, I. Cucchi, F. Y. Bruno, S. Riccò, T. K. Kim, M. Hoesch, C. Barreateau, E. Giannini, C. Besnard, A. A. Soluyanov, and F. Baumberger, Fermi Arcs and Their Topological Character in the Candidate Type-II Weyl Semimetal MoTe<sub>2</sub>, *Phys. Rev. X* **6**, 031021 (2016).
- [13] J. Jiang, Z. K. Liu, Y. Sun, H. F. Yang, C. R. Rajamathi, Y. P. Qi, L. X. Yang, C. Chen, H. Peng, C.-C. Hwang, S. Z. Sun, S.-K. Mo, I. Vobornik, J. Fujii, S. S. P. Parkin, C. Felser, B. H. Yan, and Y. L. Chen, Signature of type-II Weyl semimetal phase in MoTe<sub>2</sub>, *Nat. Commun.* **8**, 13973 (2017).
- [14] P. Deng, Z. Xu, K. Deng, K. Zhang, Y. Wu, H. Zhang, S. Zhou, and X. Chen, Revealing Fermi arcs and Weyl nodes in MoTe<sub>2</sub> by quasiparticle interference mapping, *Phys. Rev. B* **95**, 245110 (2017).
- [15] J. Sánchez-Barriga, M. G. Vergniory, D. Evtushinsky, I. Aguilera, A. Varykhalov, S. Blügel, and O. Rader, Surface Fermi arc connectivity in the type-II Weyl semimetal candidate WTe<sub>2</sub>, *Phys. Rev. B* **94**, 161401(R) (2016).
- [16] C. Wang, Y. Zhang, J. Huang, S. Nie, G. Liu, A. Liang, Y. Zhang, B. Shen, J. Liu, C. Hu, Y. Ding, D. Liu, Y. Hu, S. He, L. Zhao, L. Yu, J. Hu, J. Wei, Z. Mao, Y. Shi *et al.*, Observation of Fermi arc and its connection with bulk states in the candidate type-II Weyl semimetal WTe<sub>2</sub>, *Phys. Rev. B* **94**, 241119(R) (2016).
- [17] B. Feng, Y.-H. Chan, Y. Feng, R.-Y. Liu, M.-Y. Chou, K. Kuroda, K. Yaji, A. Harasawa, P. Moras, A. Barinov, W. Malaeb, C. Bareille, T. Kondo, S. Shin, F. Komori, T.-C. Chiang, Y. Shi, and I. Matsuda, Spin texture in type-II Weyl semimetal WTe<sub>2</sub>, *Phys. Rev. B* **94**, 195134 (2016).
- [18] A. Yu. Kitaev, Fault-tolerant quantum computation by anyons, *Ann. Phys. (Amsterdam)* **303**, 2 (2003).
- [19] C. Nayak, S. H. Simon, A. Stern, M. Freedman, and S. D. Sarma, Non-Abelian anyons and topological quantum computation, *Rev. Mod. Phys.* **80**, 1083 (2008).
- [20] F. C. Chen, X. Luo, R. C. Xiao, W. J. Lu, B. Zhang, H. X. Yang, J. Q. Li, Q. L. Pei, D. F. Shao, R. R. Zhang, L. S. Ling, C. Y. Xi, W. H. Song, and Y. P. Sun, Superconductivity enhancement in the S-doped Weyl semimetal candidate MoTe<sub>2</sub>, *Appl. Phys. Lett.* **108**, 162601 (2016).
- [21] H. Takahashi, T. Akiba, K. Imura, T. Shiino, K. Deguchi, N. K. Sato, H. Sakai, M. S. Bahramy, and S. Ishiwata, Anticorrelation between polar lattice instability and superconductivity in the Weyl semimetal candidate MoTe<sub>2</sub>, *Phys. Rev. B* **95**, 100501 (2017).
- [22] S. Cho, S. H. Kang, H. S. Yu, H. W. Kim, W. Ko, S. W. Hwang, W. H. Han, D.-H. Choe, Y. H. Jung, K. J. Chang, Y. H. Lee, H. Yang, and S. W. Kim, Te vacancy-driven superconductivity in orthorhombic molybdenum ditelluride, *2D Mater.* **4**, 021030 (2017).
- [23] M. Mandal, S. Marik, K. P. Sajilesh, Arushi, D. Singh, J. Chakraborty, N. Ganguli, and R. P. Singh, Enhancement of the superconducting transition temperature by Re doping in Weyl semimetal MoTe<sub>2</sub>, *Phys. Rev. Mater.* **2**, 094201 (2018).
- [24] Y. Li, Q. Gu, C. Chen, J. Zhang, Q. Liu, X. Hu, J. Liu, Y. Liu, L. Ling, M. Tian, Y. Wang, N. Samarth, S. Li, T. Zhang, J. Feng, and J. Wang, Nontrivial superconductivity in topological MoTe<sub>2-x</sub>S<sub>x</sub> crystals, *Proc. Natl. Acad. Sci. U.S.A.* **115**, 9503 (2018).
- [25] Z. Guguchia, F. von Rohr, Z. Shermadini, A. T. Lee, S. Banerjee, A. R. Wieteska, C. A. Marianetti, B. A. Frandsen, H. Luetkens, Z. Gong, S. C. Cheung, C. Baines, A. Shengelaya, G. Taniashvili, A. N. Pasupathy, E. Morenzoni, S. J. L. Billinge, A. Amato, R. J. Cava, R. Khasanov, and Y. J. Uemura, Signatures of the topological  $s^{+-}$  superconducting order parameter in the type-II Weyl semimetal  $T_d$ -MoTe<sub>2</sub>, *Nat. Commun.* **8**, 1082 (2017).
- [26] P. Hosur, X. Dai, Z. Fang, and X.-L. Qi, Time-reversal-invariant topological superconductivity in doped Weyl semimetals, *Phys. Rev. B* **90**, 045130 (2014).
- [27] M. Y. Zhang, Z. X. Wang, Y. N. Li, L. Y. Shi, D. Wu, T. Lin, S. J. Zhang, Y. Q. Liu, Q. M. Liu, J. Wang, T. Dong, and N. L. Wang, Light-Induced Subpicosecond Lattice Symmetry Switch in MoTe<sub>2</sub>, *Phys. Rev. X* **9**, 021036 (2019).

- [28] See Supplemental Material at <http://link.aps.org/supplemental/10.1103/PhysRevB.102.064502> for supplemental data and discussions on the sample growth and spectra analysis.
- [29] A. Gurevich, Enhancement of the upper critical field by non-magnetic impurities in dirty two-gap superconductors, *Phys. Rev. B* **67**, 184515 (2003).
- [30] I. I. Mazin, D. J. Singh, M. D. Johannes, and M. H. Du, Unconventional Superconductivity with a Sign Reversal in the Order Parameter of  $\text{LaFeAsO}_{1-x}\text{F}_x$ , *Phys. Rev. Lett.* **101**, 057003 (2008).
- [31] J. Jaroszynski, F. Hunte, L. Balicas, Y.-j. Jo, I. Raičević, A. Gurevich, D. C. Larbalestier, F. F. Balakirev, L. Fang, P. Cheng, Y. Jia, and H. H. Wen, Upper critical fields and thermally-activated transport of  $\text{NdFeAsO}_{0.7}\text{F}_{0.3}$  single crystal, *Phys. Rev. B* **78**, 174523 (2008).
- [32] G. E. Blonder, M. Tinkham, and T. M. Klapwijk, Transition from metallic to tunneling regimes in superconducting micro-constrictions: Excess current, charge imbalance, and supercurrent conversion, *Phys. Rev. B* **25**, 4515 (1982).
- [33] P. Szabó, P. Samuely, J. Kačmarčík, T. Klein, J. Marcus, D. Fruchart, S. Miraglia, C. Marcenat, and A. G. M. Jansen, Evidence for Two Superconducting Energy Gaps in  $\text{MgB}_2$  by Point-Contact Spectroscopy, *Phys. Rev. Lett.* **87**, 137005 (2001).
- [34] D. Daghero, M. Tortello, P. Pecchio, V. A. Stepanov, and R. S. Gonnelli, Point-contact Andreev-reflection spectroscopy in anisotropic superconductors: The importance of directionality, *Low Temp. Phys.* **39**, 199 (2013).
- [35] G. Sheet, S. Mukhopadhyay, and P. Raychaudhuri, Role of critical current on the point-contact Andreev reflection spectra between a normal metal and a superconductor, *Phys. Rev. B* **69**, 134507 (2004).
- [36] A. A. Golubov, A. Brinkman, Y. Tanaka, I. I. Mazin, and O. V. Dolgov, Andreev Spectra and Subgap Bound States in Multiband Superconductors, *Phys. Rev. Lett.* **103**, 077003 (2009).
- [37] D. Daghero, M. Tortello, G. A. Ummarino, and R. S. Gonnelli, Directional point-contact Andreev-reflection spectroscopy of Fe-based superconductors: Fermi surface topology, gap symmetry, and electron-boson interaction, *Rep. Prog. Phys.* **74**, 124509 (2011).
- [38] G. Deutscherr, Andreev-Saint-James reflections: A probe of cuprate superconductors, *Rev. Mod. Phys.* **77**, 109 (2005).
- [39] L. Y. L. Shen and J. M. Rowell, Zeo-Bias Tunneling Anomalies-Temperature, Voltage, and Magnetic Field Dependence, *Phys. Rev.* **165**, 566 (1968).
- [40] C. W. J. Beenakker, Quantum transport in semiconductor-superconductor microjunctions, *Phys. Rev. B* **46**, 12841(R) (1992).
- [41] B. J. van Wees, P. de Vries, P. Magnee, and T. M. Klapwijk, Excess Conductance of Superconductor-Semiconductor Interfaces due to Phase Conjugation between Electrons and Holes, *Phys. Rev. Lett.* **69**, 510 (1992).
- [42] S. Kashiwaya and Y. Tanaka, Tunnelling effects on surface bound states in unconventional superconductors, *Rep. Prog. Phys.* **63**, 1641 (2000).
- [43] S. Sasaki, M. Kriener, K. Segawa, K. Yada, Y. Tanaka, M. Sato, and Y. Ando, Topological Superconductivity in  $\text{Cu}_x\text{Bi}_2\text{Se}_3$ , *Phys. Rev. Lett.* **107**, 217001 (2011).
- [44] S. Dissanayake, C. Duan, J. Yang, J. Liu, M. Matsuda, C. Yue, J. A. Schneeloch, J. C. Y. Teo, and D. Louca, Electronic band tuning under pressure in  $\text{MoTe}_2$  topological semimetal, *npj Quantum Mater.* **4**, 45 (2019).
- [45] Y. Naidyuk, O. Kvitnitskaya, D. Bashlakov, S. Aswartham, I. Morozov, I. Chernyavskii, G. Fuchs, S.-L. Drechsler, R. Hühne, K. Nielsch, B. Büchner, and D. Efremov, Surface superconductivity in the Weyl semimetal  $\text{MoTe}_2$  detected by point contact spectroscopy, *2D Mater.* **5**, 045014 (2018).